Article:

PAPER • OPEN ACCESS

On Ohm's law in reduced plasma fluid models

To cite this article: B D Dudson *et al* 2021 *Plasma Phys. Control. Fusion* **63** 125008

View the article online for updates and enhancements.

On Ohm's law in reduced plasma fluid models

B D Dudson[1,2,*] ![ORCID]**, S L Newton**[3]**, J T Omotani**[3] ![ORCID] **and J Birch**[3,4]

[1] York Plasma Institute, Department of Physics, University of York, Heslington, York, YO10 5DQ, United Kingdom
[2] Lawrence Livermore National Laboratory, 7000 East Ave, Livermore, CA 94550, United States of America
[3] United Kingdom Atomic Energy Authority, Culham Centre for Fusion Energy, Culham Science Centre, Abingdon, Oxon, OX14 3DB, United Kingdom
[4] University of Exeter, Stocker Rd, Exeter EX4 4PY, United Kingdom

E-mail: benjamin.dudson@york.ac.uk

Abstract
Drift-reduced MHD models are widely used to study magnetised plasma phenomena, in particular for magnetically confined fusion applications, as well as in solar and astrophysical research. This letter discusses the choice of Ohm's law in these models, the resulting dispersion relations for the dynamics parallel to the magnetic field, and the implications for numerical simulations. We find that if electron pressure is included in Ohm's law, then both electromagnetic and finite electron mass effects must also be included in order to obtain physical dispersion relations. A simple modification to the plasma vorticity is also found which improves handling of low density regions, of particular relevance to the simulation of the boundary region of magnetised plasmas.

Keywords: dispersion, fluid model, tokamak edge, numerical simulation, Ohm's law

(Some figures may appear in colour only in the online journal)

1. Introduction

Drift-reduced fluid models are widely used for the study of low-frequency (relative to the ion cyclotron frequency) plasma phenomena, in relatively collisional regimes where fluid models are appropriate [1], such as the edge region of present-day tokamaks. These models have also been applied to the solar corona [2, 3] and interplanetary turbulence [4]. A wide range of models have been derived in the literature, see for example [5–19]. The basic assumption they share is that at low frequencies the cyclotron motion can be averaged over, and the plasma fluid motion perpendicular to the magnetic field described by drifts due to magnetic and electric field inhomogeneities. The electrostatic potential is often determined by enforcing quasineutrality, whilst in electromagnetic models the magnetic field perturbation is determined through Ampére and Ohm's law.

Most models are constructed to conserve an energy, either by careful selection of terms in an ordering expansion (e.g. [11, 16]), or by deriving the equations from a Lagrangian (see e.g. [13, 17]). Whilst energy conservation is important for both linear and nonlinear properties [13, 14], and usually improves the numerical stability of a model implementation, it is not the only consideration. The dispersion relation of the model, and the characteristics of the waves it supports, are less often detailed. Physically the group speed of these waves determines how fast information propagates in the system, which must not exceed the speed of light in vacuum.

---

* Author to whom any correspondence should be addressed.

In numerical implementations, the fastest waves set the CFL limit on explicit time steps, and for implicit time stepping methods [20–22] contribute to the difficulty of inverting the system Jacobian. Implementations of 3D drift-reduced fluid models for plasma turbulence applications include BOUT [23, 24], BOUT++ [25], GBS [26], TOKAM-3D [27], and STORM [28]. Each of these codes use different numerical methods, coordinate systems, and have variations in the form of equations solved, but they all share common features of drift-reduced systems: a vorticity equation, coupled to a parallel Ohm's law and a density continuity equation. Here we examine numerical issues arising from the the linear behavior of this fundamental set of equations.

This letter aims to clarify discussion of the physical completeness and numerical stability of reduced plasma fluid models, and in particular the effect of the choice of Ohm's law. Several studies employing reduced fluid models have retained both electromagnetic and electron inertia effects (e.g. [14, 26, 29, 30]) and there have been discussions of the resulting dispersion relation [10, 14, 21], but many studies do not include these terms, and the impact on the dispersion relation of the various approximations has not to our knowledge been clearly presented in one place. Therefore in section 2 we introduce the drift-reduced equations, then examine the behaviour of the electrostatic approximation in section 2.1 and move on to consider electromagnetic models in section 2.2. Section 3 illustrates the practical importance of the linear modes for time step and iteration count in example nonlinear simulations. Conclusions are given in section 4.

2. Drift-reduced MHD model dispersion relations

In this letter we consider a series of simplified drift-reduced plasma fluid models, which evolve the (electron) density n, vorticity U, and take a form for Ohm's law parallel to the magnetic field. A full derivation of the drift-reduced equations can be found elsewhere [16] and is beyond the scope of this paper. We focus for simplicity on isothermal perturbations of a uniform stationary plasma, consisting of a single ion species and electrons, in a uniform magnetic field, in the cold ion limit. We therefore do not need to include finite Larmor radius corrections to the drift motion of either species or ion viscosity. We give a brief outline of the derivation of the model, using SI units throughout except for electron temperature T_e in eV, which we follow by considering step-by-step the form of the Ohm's law. We comment on the potential impact of removing some of the simplifications considered, but a full analysis of those models is beyond the scope of the present paper.

The electron density continuity equation is used to avoid the need to evaluate high order ion polarisation velocity terms:

$$\frac{\partial n}{\partial t} = -\nabla \cdot (n\mathbf{v}_e),$$

(1)

where $\mathbf{v}_e$ is the electron fluid velocity. The quasineutrality assumption is enforced through current continuity

$$\nabla \cdot \mathbf{J} = 0,$$

(2)

and the current parallel to the magnetic field $J_{||} = \mathbf{b} \cdot \mathbf{J}$ is derived from the electron momentum equation [1]

$$m_e n \frac{d\mathbf{v}_e}{dt} + \nabla p_e + \nabla \cdot \Pi_e + en(\mathbf{E} + \mathbf{v}_e \times \mathbf{B}) = \mathbf{F},$$

(3)

where p_e is the electron pressure and $\mathbf{F}$ is the friction between electrons and ions, which will appear in the equations below as resistivity. In the drift approximation it is assumed that charged particle motion is due to parallel flow along magnetic field-lines, and drifts in the perpendicular direction. For simplicity we here neglect $E \times B$ drift (since it does not lead to charge separation) and as we assume constant background magnetic field, the diamagnetic drift is also neglected. The relevant velocity of electrons and ions would therefore be given here by the sum of parallel flow and polarisation drift: $\mathbf{v}_{i,e} = \mathbf{b} v_{||i,e} + \mathbf{v}_{i,e}^{pol}$. Note that structure induced in the solution by the drift terms, as well as the evaluation of the required field gradients, may introduce additional limitations on numerical speed and accuracy not considered here. Finally, following standard orderings, the electron polarisation drift and viscosity Π_e are neglected, as they are small in the electron mass. The ion polarisation drift is approximately given by

$$\mathbf{v}_i^{pol} \simeq \frac{m_i}{eB^2} \frac{d\mathbf{E}_\perp}{dt},$$

(4)

which arises from the time-derivative of the $E \times B$ flow velocity.

Using the Coulomb gauge, $\mathbf{E} = -\nabla \phi - \partial_t \mathbf{A}$, but following the standard low-β orderings the electromagnetic contribution to $\mathbf{E}_\perp$ is neglected, so $\mathbf{E}_\perp \simeq -\nabla_\perp \phi$. Since we are interested in the linear response only, with a stationary background, the nonlinear advection term can be dropped so that

$$\frac{d\mathbf{E}_\perp}{dt} \simeq -\frac{\partial}{\partial t} \nabla_\perp \phi.$$

(5)

Similarly we can neglect here the variation of density in the ion polarisation, sometimes called the Boussinesq approximation (see [31] and references therein) when the background is not formally uniform, so the divergence of the ion polarisation current can be written as

$$\nabla \cdot \mathbf{J}_i^{pol} = \nabla \cdot \left(en\mathbf{v}_i^{pol} \right) \simeq -\frac{m_i n_0}{B^2} \frac{\partial}{\partial t} \nabla_\perp^2 \phi,$$

(6)

where n_0 is a constant background density.

Thus we have the minimal set of reduced MHD equations which we will study in this letter:

$$\frac{\partial n}{\partial t} = -\nabla \cdot \left(\mathbf{b} n_0 v_{||e} \right),$$

(7)

$$\frac{m_i n_0}{B^2} \frac{\partial}{\partial t} \nabla_\perp^2 \phi = \nabla \cdot \left(\mathbf{b} J_{||} \right),$$

(8)

$$\frac{m_e}{e} \frac{\partial v_{||e}}{\partial t} = -\frac{1}{en_0} \partial_{||} p_e + \partial_{||} \phi + \frac{\partial A_{||}}{\partial t} + \eta J_{||},$$

(9)

$$\frac{m_i}{e} \frac{\partial v_{||i}}{\partial t} = -\partial_{||} \phi - \frac{\partial A_{||}}{\partial t} - \eta J_{||},$$

(10)

$$J_{||} = en_0 \left(v_{||i} - v_{||e} \right) = -\frac{1}{\mu_0} \nabla^2 A_{||}, \qquad (11)$$

which are essentially the same equations as used in [30–32]. Note that in the isothermal electron limit the thermal force does not appear in the expression for the parallel friction $\mathbf{b} \cdot \mathbf{F} = en_0 \eta J_{||}$, where the parallel Spitzer resistivity for a pure deuterium plasma is $\eta = 0.51 m_e/n_0 e^2 \; \tau_{ei}$ and $\tau_{ei} = 12 \pi^{3/2} m_e^{1/2} T_e^{3/2} \epsilon_0^2 /2^{1/2} n_0 e^{5/2} \ln \Lambda$ is the electron-ion collision time [33]. Note that [13], for example, gives a more complete expression for the parallel electron velocity, which reduces to (9) in the linear limit we will consider here.

With a slight modification the system of equations given above could be used to describe, approximately, modes above the ion acoustic frequency (see section 2.1.1) in a system with additional heavy ion species, whose parallel flow is negligible. The ion mass in the ion polarisation velocity would be replaced with an effective mass and an effective charge would appear in the collision time to represent the multiple species pitch-angle scattering. However, a complete representation of a multi-ion system, even in the cold ion limit, would look quite different and introduce additional numerical complexity, as individual ion continuity equations would be needed, as well as expressions for the various contributions to the inter-species friction.

The inclusion of electron inertia or pressure in Ohm's law, (9), significantly change the character of the waves in this system, as compared to ideal or resistive MHD, introducing the inertial (IAW) or kinetic Alfvén waves (KAW) [34], whose wave speeds along the magnetic field have a dependence on wave-number perpendicular to the magnetic field, $k_\perp$. In the following sections we examine the effect of approximations made to (9) on the dispersion relations, and do not note explicitly the various $\omega = 0$ solutions which arise. Here we are concerned with ensuring that the resulting wave speeds do not diverge or exceed the speed of light in vacuum c for arbitrary $k_\perp$.

In this paper we consider isothermal models with fixed electron temperature T_e, in which the right hand side of the continuity equation (7) contains a reference density n_0 rather than the evolving density n. This does not affect the linear analysis presented here, since the linearised system is unaffected by this choice for a stationary equilibrium. Nonlinearly n_0 rather than n is required in this limit so that by multiplying the set of equations (7)–(10) by $p_e = enT_e$, ϕ, $v_{||e}$ and $v_{||i}$ respectively, an energy equation can be derived:

$$\frac{\partial}{\partial t} \left[\frac{1}{2} e T_e \frac{n^2}{n_0} + \frac{1}{2} m_i n_0 \frac{|\nabla_\perp \phi|^2}{B^2} + \frac{1}{2} m_e n_0 v_{||e}^2 \right.$$
$$\left. + \frac{1}{2} m_i n_0 v_{||i}^2 + \frac{|\nabla_\perp A_{||}|^2}{2\mu_0} \right] = -\eta j_{||}^2 + \text{Div. terms} \quad (12)$$

where the left hand side represents time dependence of the internal energy, E×B flow energy, electron and ion parallel flow energy, and electromagnetic field energy. On the right is a dissipation term due to resistivity, and divergence terms which become boundary fluxes when integrated over the domain. In a

non-isothermal model the density equation would not participate in the energy balance, and could contain the evolving density n rather than constant n_0; the equations above would in that case be augmented by an internal energy (pressure) equation for the electrons.

The modifications to Ohm's law made in the following sections will modify the conserved energy on the left of (12), while retaining its general form: In the electrostatic approximation (section 2.1) the $A_{||}$ term will be removed; if ion flow is neglected then the ion parallel kinetic energy is removed; while if electron mass is neglected then the electron parallel kinetic energy is removed. We note that in more complete models with advection and other cross-field energy transfer terms, modifications to one equation must typically be accompanied by changes to other equations, so as to avoid breaking the energy conservation properties of a model.

2.1. Electrostatic model

In the case of isothermal electrons with constant temperature T_e

$$\frac{1}{en} \partial_{||} p_e \to \frac{T_e}{n_0} \partial_{||} n. \qquad (13)$$

Neglecting both the electromagnetic part of the electric field and the electron mass, Ohm's law (9) then reduces to

$$\eta J_{||} = -\partial_{||}\phi + \frac{T_e}{n_o} \partial_{||} n, \qquad (14)$$

so that in the limit of $\eta \to 0$ the well known Boltzmann relationship between potential ϕ and density n is recovered. For clarity we start by neglecting the ion parallel flow, and so exclude the parallel ion sound wave—we reintroduce it and consider its effect in section 2.1.1. The parallel current can then be written as $J_{||} = -env_{||e}$. Linearising the set of equations (7)–(9), with

$$\partial_{||} \to ik_{||}, \qquad \frac{\partial}{\partial t} \to -i\omega, \qquad \nabla_\perp^2 \to -k_\perp^2, \qquad (15)$$

the dispersion relation with finite resistivity is then given by

$$-i\omega = -k_{||}^2 \frac{T_e}{\eta en_0} \left(\frac{1}{k_\perp^2 \rho_s^2} + 1 \right). \qquad (16)$$

Here $\rho_s = c_s/\Omega_i = \sqrt{T_e m_i/eB^2}$ is the hybrid ion or ion sound gyroradius, where $c_s = \sqrt{eT_e/m_i}$ is the ion sound speed and Ω_i is the ion cyclotron frequency. Typical magnetised plasma edge turbulence, for example in tokamaks and linear devices, have scale lengths perpendicular to the magnetic field such that $k_\perp \rho_s \sim 0.1 - 1$.

Equation (16) represents a diffusion equation along the magnetic field for the evolving quantities (n, ϕ, or $J_{||}$) with diffusion coefficient D:

$$D = \frac{T_e}{\eta en_0} \left(\frac{1}{k_\perp^2 \rho_s^2} + 1 \right). \qquad (17)$$

Smaller $k_\perp$ modes (longer perpendicular wavelength) diffuse along the magnetic field faster than high $k_\perp$ modes. With the Spitzer resistivity $\eta \simeq 10^{-4} \ln \Lambda T_e^{-3/2}\ \Omega$m for a pure deuterium plasma:

$$D \simeq 1.3 \times 10^6 \left(\frac{T_e}{10\ \text{eV}} \right)^{5/2} \left(\frac{10^{18}\ \text{m}^{-3}}{n_0} \right)$$
$$\times \left(\frac{1}{k_\perp^2 \rho_s^2} + 1 \right)\ \text{m}^2\ \text{s}^{-1}.$$

This fast diffusion can place limits on explicit time steps or make the linear system solved for an implicit time step extremely ill conditioned, becoming more restrictive as the electron temperature increases or the system size increases (smallest $k_\perp$ decreases). Note that there is no limit to the speed at which information propagates in this model: $k_\perp = 0$ modes communicate instantaneously along magnetic field lines.

If we keep finite electron mass in Ohm's law, but still drop the electromagnetic term then (9) becomes

$$\eta J_{||} = -\partial_{||}\phi + \frac{1}{en_0}\partial_{||}p_e + \frac{m_e}{e}\frac{\partial v_{||e}}{\partial t}, \qquad (18)$$

giving the dispersion relation

$$\omega^2 + i\omega\eta \frac{v_{te}^2}{\mu_0 V_A^2 \rho_s^2} = k_{||}^2 v_{te}^2 \left(1 + \frac{1}{k_\perp^2 \rho_s^2} \right), \qquad (19)$$

where $v_{te} = \sqrt{eT_e/m_e}$ is the electron thermal speed. The second term on the left here accounts for perpendicular magnetic diffusion due to the parallel resistivity, which results from the electron–ion collisions which have a characteristic timescale $0.51/\tau_{ei} = \eta n_0 e^2/m_e = \eta \omega_{pe}^2/\mu_0 c^2 = \eta v_{te}^2/\mu_0 V_A^2 \rho_s^2$. The plasma skin depth is c/ω_{pe}, with c the speed of light in vacuum, $\omega_{pe} = \sqrt{n_0 e^2/\epsilon_0\, m_e}$ the plasma frequency, while the Alfvén speed $V_A = B/\sqrt{\mu_0 m_i n_0}$ is introduced in the last form by noting the characteristic perpendicular lengthscale of the system is the sound gyroradius. Rather than a diffusion equation, as (16), the system dispersion relation is now a wave equation. Writing the solution as $\omega = \omega_0 + i\gamma$, where ω_0 and γ are real,

$$\omega_0 = \frac{k_{||}}{k_\perp}\frac{v_{te}}{\rho_s}\sqrt{1 + k_\perp^2\ \rho_s^2 - \frac{\eta^2}{4}\frac{k_\perp^2}{k_{||}^2}\frac{v_{te}^2}{\mu_0^2 V_A^4 \rho_s^2}},$$
$$\gamma = -\frac{\eta}{2}\frac{v_{te}^2}{\mu_0 V_A^2\ \rho_s^2} = -\frac{0.51}{2\tau_{ei}}. \qquad (20)$$

As we are considering the fluid limit, the collision frequency must be faster than the other timescales in the system, so these waves must damp rapidly. The same problem is encountered however: the wave speed diverges as $k_\perp \to 0$.

Neglecting resistivity, in the cold plasma limit $T_e = 0$, the dispersion relation (19), reduces to

$$\omega^2 = \Omega_i^2 \frac{k_{||}^2}{k_\perp^2}\frac{m_i}{m_e}. \qquad (21)$$

This is the electrostatic wave which has been noted in the context of gyrokinetic simulations to limit the timestep, see for example the early discussion by Lee [35] or a recent case by McMillan [36].

These fast waves present a problem for global plasma simulations, where the largest perpendicular scale is much greater than ρ_s: As the system size increases, the fastest wave speed will rapidly increase, and for (semi-)implicit methods the problem will become increasingly poorly conditioned.

2.1.1. Ion parallel momentum.
If the ion parallel momentum is also evolved, in the electrostatic approximation, (10) gives

$$\frac{m_i}{e}\frac{\partial v_{||i}}{\partial t} = -\partial_{||}\phi - \eta J_{||}, \qquad (22)$$

and the dispersion relation becomes

$$\omega^2 + i\omega\eta \frac{v_{te}^2}{\mu_0 V_A^2 \rho_{sm}^2}\left(1 - \frac{k_{||}c_{sm}^2}{\omega^2} \right)$$
$$= \frac{k_{||}^2 v_{te}^2}{k_\perp^2 \rho_{sm}^2}\left(1 + k_\perp^2 \rho_{sm}^2 - \frac{k_{||}^2 c_{sm}^2}{\omega^2} \right), \qquad (23)$$

where for convenience we have defined the electron mass corrections $c_{sm}^2 = c_s^2/(1 + m_e/m_i)$ and $\rho_{sm} = c_{sm}/\Omega_i$. Neglecting the electron mass, in the limit of zero resistivity, this reduces to simply the bracket on the right equal to zero

$$\omega^2 = k_{||}^2 c_s^2 \frac{1}{\left(1 + k_\perp^2 \rho_s^2 \right)},$$

and we see that we have introduced the ion acoustic wave $\omega^2 = k_{||}^2 c_s^2$ to the system, including finite sound radius corrections when $k_\perp \neq 0$. This wave can be destabilised in the presence of background plasma gradients to give the slab branch of drift waves. Note that if we retained an isothermal ion pressure term in (22) we would recover the dispersion relation from (23) with the simple modification $c_{sm}^2 \to c_{sm}^2(1 + T_i/T_e)$. This also holds for the electromagnetic result (26) which is discussed in the next section.

Neglecting only the electron mass in (23), we see the ion sound radius couples the diffusive mode and the ion acoustic wave at finite $k_\perp$. When $\omega^2 \gg k_{||}^2\ c_s^2$ the parallel ion momentum equation can be neglected, and we recover $-i\omega\eta = -\mu_0 k_{||}^2 V_A^2 \rho_s^2 (1 + k_\perp^2\ \rho_s^2)/k_\perp^2\ \rho_s^2$, that is the diffusive mode (16). By comparing the diffusive timescale to the inverse ion acoustic frequency, we see that this limit corresponds as expected to the case of $m_i \to \infty$, or $k_\perp \to 0$ at finite $k_{||}$.

The parallel ion momentum evolution modifies the electrostatic wave described by (21) simply by multiplying the right hand side of that relation by $(1 + m_e/m_i)$. The modified frequencies of the resistive wave solution (20) are

$$\omega_0 = \frac{k_{||}}{k_\perp}\frac{v_{te}}{\rho_s}\sqrt{1 + k_\perp^2\ \rho_s^2 + \frac{m_e}{m_i} - \frac{\eta^2}{4}\frac{k_\perp^2}{k_{||}^2}\frac{v_{te}^2}{\mu_0^2 V_A^4 \rho_s^2}\left(1 + \frac{m_e}{m_i} \right)^2},$$
$$\gamma = -\frac{0.51}{2\tau_{ei}}\left(1 + \frac{m_e}{m_i} \right).$$

Thus the parallel ion momentum evolution has not removed the difficulty as $k_\perp \to 0$.

Several other physical effects could limit the rate at which these electrostatic waves propagate. For example, we have made an isothermal approximation in relating electron pressure p_e to density n, which would break down for sufficiently fast phenomena—but we should remain in the collisional limit. We have considered the cold ion limit for simplicity, formally requiring the ion temperature smaller than T_e by the mass ratio. However experimental results show that the ion temperature is often comparable to or larger than T_e [37, 38], so finite ion Larmor radius effects should introduce further dispersion. Here, however, we focus on Ohm's law, where a partial solution to the problem of unphysically fast waves is known to result from retaining electromagnetic effects [35]. This introduces the Alfvén wave and is discussed in the next section.

2.2. Electromagnetic model

Now we examine the dispersion relation of the system retaining the electromagnetic contribution to the parallel electric field. We retain the the parallel ion momentum evolution, noting from the electrostatic case the relatively straightforward changes it introduced. Again we begin by neglecting the finite electron mass, which gives the dispersion relation

$$\omega^2 + i\omega\eta\frac{k^2}{\mu_0}\left(1 - \frac{k_\parallel^2 c_s^2}{\omega^2}\right)$$
$$= k_\parallel^2 V_A^2\left[\frac{k^2}{k_\perp^2} + k^2\rho_s^2 + \frac{k_\parallel^2 c_s^2}{\omega^2}\left(\frac{\omega^2}{k_\parallel^2 V_A^2} - \frac{k^2}{k_\perp^2}\right)\right]. \quad (24)$$

Note that this relation does not diverge as $k_\perp \to 0$, unlike the electrostatic relation in (16), which we see by multiplying through by $k_\perp$, then letting $k_\perp \to 0$ and $k^2 \to k_\parallel^2$. Including the electromagnetic term can therefore improve numerical stability. However, the equation now has a problem at high $k_\perp$: the parallel wave speed increases with $k_\perp$. Neglecting the resistivity and taking low $\beta = c_s^2/V_A^2$ so the ion acoustic wave can be neglected, we see that this is due to the kinetic Alfvén wave with dispersion relation

$$\omega^2 = k_\parallel^2 V_A^2\left(1 + k_\perp^2\rho_s^2\right); \quad (25)$$

the origin of the $k_\perp^2\rho_s^2$ term is the $\partial_\parallel p_e$ term in Ohm's law.

Typical blob or turbulence simulations need to resolve smallest scales of around $\delta_x \sim \rho_s$, so the highest $k_\perp$ in the simulation has $k_\perp = 2\pi/\delta_x \sim 10/\rho_s$. Adding this term therefore introduces a wave into the system around 10 times faster than the Alfvén speed. For deuterium plasmas in a 1 T magnetic field, this wave will exceed the speed of light once the density falls below $n_0 \sim 2.6 \times 10^{17}$ m^{-3}. This can quite easily occur in plasma edge simulations whose domain often includes a near-vacuum region such as the far scrape-off layer (SOL) in tokamak simulations.

Going on to include finite electron mass, the dispersion relation becomes

$$\omega^2\left(1 + \frac{k^2 c^2}{\omega_{pe}^2}\frac{1}{\left(1 + \frac{m_e}{m_i}\right)}\right) + i\omega\eta\frac{k^2}{\mu_0}\left(1 - \frac{k_\parallel^2 c_{sm}^2}{\omega^2}\right)$$
$$= k_\parallel^2 V_A^2\left[\frac{k^2}{k_\perp^2} + k^2\rho_{sm}^2 + \frac{k_\parallel^2 c_{sm}^2}{\omega^2}\left(\frac{\omega^2}{k_\parallel^2 V_A^2} - \frac{k^2}{k_\perp^2}\right)\right], \quad (26)$$

where we note we could rewrite the skin depth contribution as $k^2 c^2/\omega_{pe}^2 = k^2 \rho_s^2\ V_A^2/v_{te}^2$. (If the common approximation to Ampère's law in the strongly magnetised limit $\mu_0 j_\parallel \approx -\nabla_\perp^2 A_\parallel$ is used, $k \to k_\perp$ in (24) and (26)). Equation (26) is well behaved at large perpendicular length scales $k_\perp \to 0$: neglecting resistivity and finite electron mass, the ρ_{sm} contribution $\to 0$ with $k_\perp$ and we recover the decoupled shear Alfvén and ion acoustic waves, as noted in [14]: $\left(\omega^2 - k_\parallel^2 V_A^2 k^2/k_\perp^2\right)\left(\omega^2 - k_\parallel^2\ c_s^2\right) = 0$. Equation (26) is also now well behaved when $k_\perp$ becomes large. We can first see this by considering the cold plasma limit, neglecting resistivity: only the first term on the right hand side survives, and we obtain the electromagnetic modification of (21) [35]

$$\frac{\omega^2 k^2 m_e}{\Omega_i^2 k_\parallel^2 m_i} + \left(1 + \frac{m_e}{m_i}\right)\left(\frac{\omega^2}{k_\parallel^2 V_A^2} - \frac{k^2}{k_\perp^2}\right) = 0,$$

which leads to the inertial Alfvén wave dispersion relation,

$$\omega^2 = k_\parallel^2 V_A^2 \left/ \left[\frac{k_\perp^2}{k^2} + \frac{k_\perp^2 c^2}{\omega_{pe}^2}\frac{1}{\left(1 + \frac{m_e}{m_i}\right)}\right].\right. \quad (27)$$

(It can be of interest to note that in the standard notation of Stix [39] this result corresponds to the full solution $Sk_\perp^2 c^2 + Pk_\parallel^2 c^2 - PS\omega^2 = 0$, unlike the quasi-electrostatic mode discussed there which neglects the PS coupling term.)

Now neglecting only the acoustic wave corrections in (26) for simplicity, we find that the modified frequencies of the resistive wave solution (20) are

$$\omega_0^2 = k_\parallel^2\ V_A^2\ \frac{\left(\frac{k^2}{k_\perp^2} + k_\perp^2\rho_s^2\right)}{\left(1 + \frac{k^2 c^2}{\omega_{pe}^2}\frac{1}{\left(1 + \frac{m_e}{m_i}\right)}\right)}$$
$$\times \left[1 - \frac{\eta^2 k^4}{4\mu_0^2 k_\parallel^2\ V_A^2}\frac{1}{\left(1 + \frac{k^2 c^2}{\omega_{pe}^2}\frac{1}{\left(1 + \frac{m_e}{m_i}\right)}\right)\left(\frac{k^2}{k_\perp^2} + k_\perp^2\rho_s^2\right)}\right], \quad (28)$$

$$\gamma = -\frac{\eta k^2}{2\,\mu_0} \frac{1}{\left(1 + \frac{k^2 c^2}{\omega_{\text{pe}}^2} \frac{1}{\left(1 + \frac{m_e}{m_i}\right)}\right)}, \qquad (29)$$

when the term in the square bracket is positive, for example at low $k_\perp$. Upon neglecting resistivity, this recovers the standard dispersion relation [34] describing the combination of inertial ($T_e \to 0$) and kinetic Alfvén waves

$$\omega_0^2 = k_\parallel^2\, V_A^2\, \left(\frac{k^2}{k_\perp^2} + k_\perp^2 \rho_s^2\right) \Big/ \left(1 + \frac{k^2 c^2}{\omega_{\text{pe}}^2} \frac{1}{\left(1 + \frac{m_e}{m_i}\right)}\right),$$

which reduces in the large $k_\perp$ limit to a wave with electron thermal speed, $\omega_0^2 \to k_\parallel^2\, v_{\text{te}}^2$. Returning to (26) to consider the limit of finite resistivity and high $k_\perp$, the ω_{pe}, resistive and ρ_{sm} terms dominate and we recover the well-behaved form as in (19),

$$\omega^2 + i\omega\eta \frac{v_{\text{te}}^2}{\mu_0\, V_A^2\, \rho_s^2} = k_\parallel^2 v_{\text{Te}}^2, \qquad (30)$$

which has the approximate strongly damped solution at large collisionality $\omega \approx -i(0.51/\tau_{\text{ei}}) + (k_\parallel^2 v_{\text{te}}^2 \tau_{\text{ei}}/0.51)$.

Note that we do not need to include relativistic corrections to the electron mass in order to limit the wave speed, except in the cases where v_{te} or V_A exceed c. The former occurs at $T_e > 500$ keV so would not be relevant to plasma edge simulations, but the latter occurs at $n_0 < 0.66 \times 10^{17}$ m^{-3} for a magnetic field of 5 T, so may become an issue when simulating the edge of large fusion devices.

2.2.1. Space charge effects and displacement current.

It is reasonable to suppose that if a wave is found which exceeds the speed of light, then we should re-examine the approximations made to Maxwell's equations in deriving the reduced MHD equations. In this section we therefore consider the effect of including space charges (breakdown of quasi-neutrality), and then displacement current.

The vorticity equation arises from current continuity, (2), under the quasi-neutrality assumption, that is the charge density $\rho \simeq 0$. This assumption may break down at small scales and low densities, and charge continuity becomes

$$\nabla \cdot \mathbf{J} = -\frac{\partial \rho}{\partial t} = \epsilon_0 \nabla^2 \frac{\partial \phi}{\partial t}, \qquad (31)$$

where the Coulomb gauge $\nabla \cdot \mathbf{A} = 0$ is used here. This modifies the vorticity equation equation (8) to:

$$\frac{\partial U}{\partial t} = \nabla \cdot \left(\mathbf{b} J_\parallel\right), \qquad U \simeq \frac{m_i n_0}{B^2} \nabla_\perp^2 \phi + \epsilon_0 \nabla^2 \phi, \qquad (32)$$

where the vorticity U has been defined to include the space charge term and can be written as:

$$U = \frac{1}{\mu_0} \left(\frac{1}{V_A^2} \nabla_\perp^2 \phi + \frac{1}{c^2} \nabla^2 \phi\right). \qquad (33)$$

This results in the dispersion relation, neglecting finite electron mass and ion acoustic effects:

$$\omega^2 + i\omega\eta \frac{k^2}{\mu_0} = k_\parallel^2 V_A^2 \frac{k^2}{k_\perp^2} \left[\frac{c^2}{c^2 + V_A^2 \left(k^2/k_\perp^2\right)} + k_\perp^2 \rho_s^2\right], \quad (34)$$

Equation (34) suggests a way to limit the shear Alfvén waves to less than light speed at low density, which will be explored further in section 4. It does not however solve the problem at high $k_\perp$, and waves with arbitrarily high group speed along the magnetic field are still supported.

Since we are not evolving the perpendicular components of the vector potential **A**, displacement currents in the perpendicular direction are not included here: they would modify the perpendicular components of **A**, but do not lead to motion of charges, and so would not modify charge continuity (vorticity). As we are explicitly evolving only the parallel component of the displacement current, but not the parallel component of the magnetic field, the ordinary light wave will not appear in the dispersion relation. Ampère's law keeping only $A_\parallel$ and including the displacement current becomes

$$J_\parallel = -\frac{1}{\mu_0} \nabla^2 A_\parallel + \epsilon_0\, \frac{\partial}{\partial t} \partial_\parallel \phi + \epsilon_0\, \frac{\partial^2 A_\parallel}{\partial t^2}. \qquad (35)$$

Continuing to retain space charge, the vorticity equation becomes

$$\omega \left[\left(\frac{m_i n_0}{B^2} + \epsilon_0\right) k_\perp^2 + \epsilon_0 k_\parallel^2\right] \phi = k_\parallel \left(\frac{k_\perp^2}{\mu_0} - \omega^2 \epsilon_0\right) A_\parallel$$
$$+ k_\parallel^2 \epsilon_0 \omega \phi. \qquad (36)$$

Note that the $\epsilon_0\, k_\parallel^2$ term on the left (from space charge) cancels with the same term on the right (from displacement current). The dispersion relation then becomes

$$\omega^2 + i\omega\eta \frac{k^2}{\mu_0} \left(1 - \frac{\omega^2}{k^2 c^2}\right)$$
$$= k_\parallel^2 V_A^2 \frac{k^2}{k_\perp^2} \left[\frac{c^2}{c^2 + V_A^2 \left(k^2/k_\perp^2\right)} + k_\perp^2 \rho_s^2 \left(1 - \frac{\omega^2}{k^2 c^2}\right)\right], \quad (37)$$

which at large $k_\perp$ without resistivity leads to the same wave as when displacement current is not included, (34). This means that these equations can have waves with speeds (both group and phase) along the magnetic field greater than the speed of light, without including the electron mass. However, we see that including the parallel displacement current is not essential to provide effective limitation of the wave speeds in low density regions.

For ease of reference, the low and high $k_\perp$ limits of the dispersion relations presented in this section are summarised in the appendix, table A1.

3. Nonlinear timestep benchmark

To demonstrate the practical importance of the various dispersion relations derived above, we benchmark nonlinear
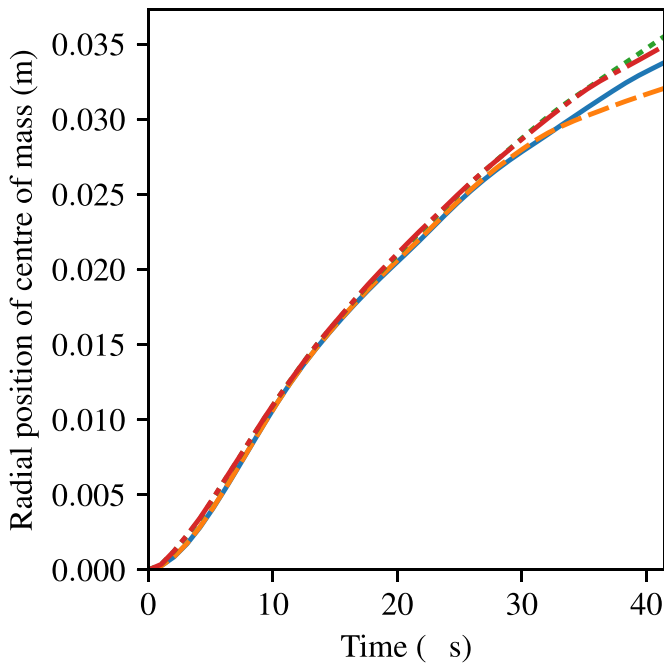
Figure 1. Radial position of the filament centre of mass for electrostatic, zero electron mass (blue solid); electrostatic, finite electron mass (orange dashed); electromagnetic, zero electron mass (green dotted); and electromagnetic, finite electron mass (red dash-dotted) cases.

simulations using different versions of Ohm's law. We use STORM [28, 40], which is typical of BOUT++ drift-reduced fluid models, and choose as a test case a simulation of an isolated scrape-off layer (SOL) filament, in simplified slab geometry, based on the cold-ion case in [41]. Isolated filament simulations have a moderate computational cost but include important features of edge/SOL turbulence simulations, being highly non-linear and including sheath boundary conditions. More details of the model and simulation setup are given in appendix B and ref. [42].

We compare electrostatic and electromagnetic models both neglecting and including electron inertia. The evolution of the filaments simulated with these four different models are essentially identical, due to the very low $\beta \approx 2.6 \times 10^{-4}$ in the L-mode SOL conditions of our test case, as shown for example by the radial position of the centre of mass in figure 1. The slight difference visible between electrostatic and electromagnetic models originates in a small transient at the start of the simulations as the parallel current develops from the initial value of zero, which happens almost instantly in the electrostatic simulations, but at the speed of the Alfvén wave in the electromagnetic simulations.

BOUT++ simulations usually use the CVODE implicit time solver from the SUNDIALS suite [43], as the simulations shown in this section do, so do not have a strict Courant-Friedrichs-Lewy (CFL) constraint [44] on the time step, as would be the case if an explicit scheme were used. However, CVODE adapts the time step used to satisfy relative and absolute tolerance criteria while aiming to minimise the number of iterations, so the resulting time step is related to the

frequency of the fastest mode in the system, as we will now describe.

We compare the mode frequencies from the dispersion relations presented with the internal time step, number of iterations per time step and wall-clock time from the simulations, given in table 1. The analytical mode frequencies are evaluated using the background parameters at the midplane of the simulations. The maximum parallel wavenumber present in the simulations $k_{\parallel,max} = 2\pi/2\Delta_{\parallel}$ is the shortest wavelength that can be represented without aliasing on a grid with parallel spacing $\Delta_{\parallel}$. Similarly the maximum perpendicular wavenumber $k_{\perp,max} = 2\pi/2\Delta_{\perp}$ is set by the perpendicular grid spacing $\Delta_{\perp}$, while the minimum perpendicular wavenumber is set by the box size $k_{\perp,min} = 2\pi/L_{\perp}$. The maximum damping rate for the resistive, diffusive mode (16) in the electrostatic, zero electron inertia model and the maximum frequency (20) for the electrostatic, finite electron inertia model are evaluated with $k_{\perp,min}$. For the electromagnetic, finite electron inertia model (28) also uses $k_{\perp,min}$, as for the parameters of this test the Alfvén speed is higher than the electron thermal speed and we also evaluate it with $k \approx k_{\perp}$ for consistency with the implemented model. The maximum frequency for the kinetic Alfvén wave (25) is evaluated with $k_{\perp,max}$. We see that the average time steps taken by CVODE in the simulations are ordered as the inverse mode frequencies, table 1, and the time step and number of iterations per step are fairly consistent in all phases of the simulation, figure 2. The time steps for both electrostatic and electromagnetic models with finite electron mass are slightly smaller than the inverse mode frequencies (by a factor between 2 and 3), as would be expected when the simulations are resolving these waves.

The time step for the strongly damped electrostatic, zero electron mass model is 100 times longer than the inverse of the damping rate (16), showing that the implicit time-solver algorithm used by CVODE is able to step over this mode. The time step is nearly as long as in the electrostatic, finite electron mass case, although significantly more iterations per time step are required, leading to a wall-clock time that is three times longer.

The time step in the electromagnetic, zero electron mass case is slightly longer than the inverse of the maximum mode frequency. Note that this is the maximum $k_{\perp}$ mode, which will be most affected by numerical dissipation since its wavelength is at the grid scale, and also by collisional dissipation present in the STORM model that was not included in the analytic dispersion relation, so the mode may be expected to have a significant damping rate. It seems that this damping is enough for CVODE to step over the frequency of this mode, at the cost of a higher number of iterations per step than required for the electromagnetic, finite electron inertia model.

The electromagnetic, finite electron inertia model as implemented in STORM requires an additional inversion to solve Ampère's law for the parallel velocities and $A_{\parallel}$ [41], which is not required in the electromagnetic, zero electron inertia model where Ohm's law evolves $A_{\parallel}$ directly. Such inversions are typically a significant part of the run-time of BOUT++ simulations, here taking 13% of the run time for the electromagnetic, zero electron inertia model, and 36% for the electromagnetic,

Table 1. The time step, iteration count and wall-clock time for electrostatic (ES) and electromagnetic (EM) models compared to the analytic mode frequency $|\omega_{\text{analytic}}|$. Equation number for the dispersion relation evaluated for $|\omega_{\text{analytic}}|$ given in the DR column.

Model	DR	$1/|\omega_{\text{analytic}}|$ (ns)	Time step (ns)	Iterations/step	Wall-clock time (h)
ES, zero-m_e	(16)	0.00991	0.828	8.76	30.4
ES, finite-m_e	(20)	2.47	0.899	3.64	11.5
EM zero-m_e	(25)	3.18	7.31	6.41	3.21
EM, finite-m_e	(28)	25.8	9.25	4.35	2.36
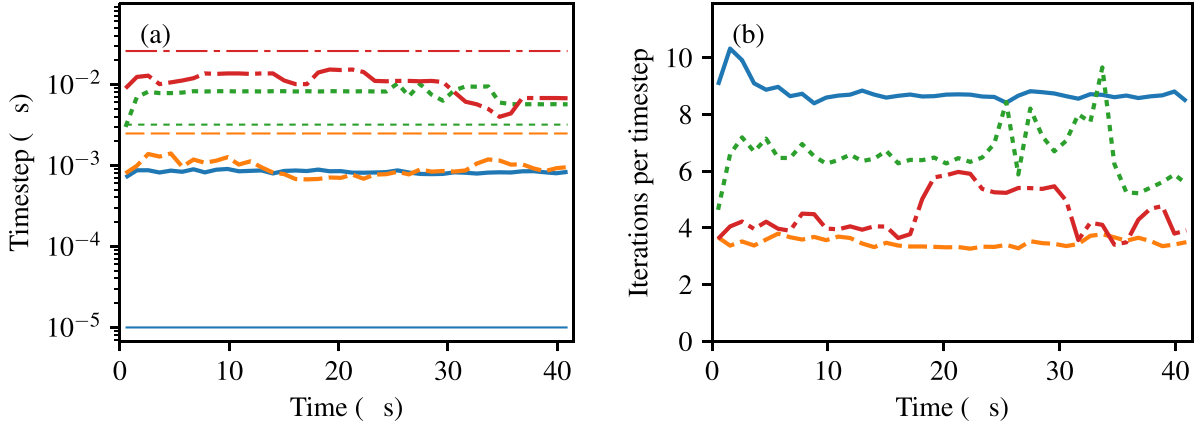
Figure 2. (a) Internal time step (thick lines) and magnitude of the inverse linear mode frequency (thin, horizontal lines) and (b) number of RHS evaluations per internal time step for electrostatic, zero electron mass (blue solid, using (16)); electrostatic, finite electron mass (orange dashed, using (20)); electromagnetic, zero electron mass (green dotted, using (25)); and electromagnetic, finite electron mass (red dash-dotted, using (28)) cases.

finite electron inertia model. Despite this, the wall-clock time for the electromagnetic, finite electron inertia model is shorter than the zero electron inertia model by a factor of 0.74, due to the longer time step and lower number of iterations per step.

4. Conclusion

We have presented a linear analysis of electrostatic and electromagnetic waves supported by a minimal drift-reduced fluid model. Though simplified, equations (7)–(9) contain the key features of a wide class of models which are used in the plasma community. This analysis sheds light on the observation that once parallel electron pressure gradients are included in Ohm's law, electrostatic simulations often encounter difficulties.

We recognise the origin of this as dispersion relations which diverge at small $k_\perp$. If finite electron mass is not included then this appears as parallel diffusion which becomes faster as $1/k_\perp^2$, whilst if finite electron mass is included then a parallel wave is found whose speed increases like $1/k_\perp$. Use of an electromagnetic Ohm's law without electron mass removes the difficulty at small $k_\perp$, but leads to unphysical behavior due to kinetic Alfvén waves at large $k_\perp$, resulting in wave speeds which increase with $k_\perp$ without limit.

A system using an electromagnetic Ohm's law with finite electron mass is found to be well behaved, with parallel wave speeds limited by the Alfvén speed at low $k_\perp$ and the electron thermal speed at high $k_\perp$, as discussed in [14]. Retaining electromagnetic terms is therefore important for limiting

the speed of waves in the system, and we have demonstrated that this can reduce the computational cost of nonlinear simulations by allowing longer time steps to be taken at acceptable iteration counts, even in the very low beta conditions of the L-mode SOL. Elsewhere, it has been found numerically that electromagnetic effects can modify the propagation and stability of plasma blobs [30] and turbulence [14] by slowing parallel wave propagation. It has also been previously noted [13] that the electrostatic approximation can lead to inconsistencies and incorrect results even at low β.

Plasma edge simulations can include low density regions, resulting in the Alfvén velocity exceeding the speed of light. Adding ϵ_0 to the perpendicular Laplacian term in the vorticity limits V_A to be slower than the speed of light, and can be easily added to existing code. This gives the modified equations:

$$\frac{\partial n}{\partial t} = -\nabla \cdot \left(\mathbf{b} n_0\, v_{||e} \right), \qquad (38)$$

$$\nabla \cdot \left(\frac{m_i n_0}{B^2} \frac{d\nabla_\perp \phi}{dt} + \epsilon_0 \frac{\partial}{\partial t} \nabla_\perp \phi \right) = \nabla \cdot \left(\mathbf{b} J_{||} \right), \quad (39)$$

$$\frac{m_e}{e} \frac{\partial v_{||e}}{\partial t} - \frac{\partial A_{||}}{\partial t} = -\frac{1}{en_0} \partial_{||} p_e + \partial_{||} \phi + \eta J_{||}, \quad (40)$$

$$J_{||} = -\frac{1}{\mu_0} \nabla_\perp^2 A_{||}, \qquad (41)$$

which have the dispersion relation:

$$\omega^2 \left(1 + \rho_s^2 k_\perp^2 \frac{V_A^2}{v_{te}^2}\right) + i\omega \frac{k_\perp^2 \eta}{\mu_0} = k_{||}^2 V_A^2 \left[\frac{c^2}{c^2 + V_A^2} + k_\perp^2 \rho_s^2\right].$$

(42)

This is now well behaved at high and low $k_\perp$, and in low density regions. Adding the $\epsilon_0 \nabla_\perp \phi$ term to the vorticity will have the effect of including the perpendicular electric field energy $\epsilon_0 E_\perp^2$ into the conserved energy of the system, but does not introduce a new transfer channel. This will have the effect of bounding the total energy in perpendicular electric fields, and so may improve numerical stability. In addition we find that the parallel part of $\epsilon_0 \nabla^2$ does not need to be included in (39), and does not provide a way to introduce parallel coupling into the vorticity equation. This is because it cancels with the displacement current in the divergence of parallel current as discussed in section 2.2.1.

Data availability statement

Acknowledgments

Appendix A. Summary of limits

Table A1. Leading order terms in the low and high $k_\perp$ limits of the dispersion relations presented in this paper, neglecting resistivity and taking $k_\parallel \ll k_\perp$ so that $k^2/k_\perp^2 \approx 1$. The column headings m_e and c_s denote whether electron mass and ion acoustic terms, respectively, are included. $\mathbf{k}_\perp$ terms leading to divergence are highlighted in bold.

Model	m_e?	c_s?	$k_\perp \to 0$	$k_\perp \to \infty$
Electrostatic (19)	✓	✗	$\omega^2 = k_\parallel^2 v_{\text{te}}^2/\mathbf{k}_\perp^2 \rho_s^2$	$\omega^2 = k_\parallel^2 v_{\text{te}}^2$
Electrostatic (23)	✓	✓	$\omega^4 = \left(\omega^2 - k_\parallel^2 c_{\text{sm}}^2\right) k_\parallel^2 v_{\text{te}}^2/\mathbf{k}_\perp^2 \rho_{\text{sm}}^2$	$\omega^2\left(\omega^2 - k_\parallel^2 v_{\text{te}}^2\right) = 0$
Electromagnetic (24)	✗	✓	$\left(\omega^2 - k_\parallel^2 V_A^2\right)\left(\omega^2 - k_\parallel^2 c_s^2\right) = 0$	$\omega^2\left(\omega^2 - k_\parallel^2 V_A^2\, \mathbf{k}_\perp^2 \rho_s^2\right) = 0$
Electromagnetic (26)	✓	✓	$\left(\omega^2 - k_\parallel^2 V_A^2\right)\left(\omega^2 - k_\parallel^2 c_{\text{sm}}^2\right) = 0$	$\omega^2\left(\omega^2 - k_\parallel^2 v_{\text{te}}^2\right) = 0$
Electromagnetic with space charge (34)	✗	✗	$\omega^2 = k_\parallel^2 V_A^2 c^2/\left(c^2 + V_A^2\right)$	$\omega^2 = k_\parallel^2 V_A^2\, \mathbf{k}_\perp^2 \rho_s^2$
Electromagnetic with ∥ displacement current, space charge (37)	✗	✗	$\omega^2 = \dfrac{k_\parallel^2\ V_A^2 c^2}{\left(c^2 + V_A^2\right)\left(1 + k_\parallel^2\ V_A^2\ \rho_s^2/c^2\right)}$	$\omega^2 = \dfrac{k_\parallel^2\ V_A^2\ \mathbf{k}_\perp^2\ \rho_s^2}{\left(1 + k_\parallel^2\ V_A^2\ \rho_s^2/c^2\right)}$
Electromagnetic with perp. space charge (42)	✓	✗	$\omega^2 = k_\parallel^2\ V_A^2 c^2/\left(c^2 + V_A^2\right)$	$\omega^2 = k_\parallel^2\ v_{\text{te}}^2$

In this appendix we collect the asymptotic limits of the dispersion relations presented above.

Appendix B. Filament simulations

In this appendix we briefly describe the STORM model and simulation setup used for the nonlinear seeded filament simulations discussed in section 3. For more details see the cold ion model in [41], and the setup for the simulation shown in figure 1(a) there, which is identical to the electromagnetic, finite electron mass case here. Simulation inputs and post-processing scripts needed to reproduce the figures in this paper are available in Zenodo at https://doi.org/10.5281/zenodo.5525078.

B.1. Models

The STORM model was originally electrostatic, with finite electron mass [28]. An electromagnetic, finite electron mass variant was described in [45]. Our test case is based on the cold ion reference case from [41], which introduced hot ion effects to the electromagnetic, finite electron mass model. For this benchmark we have implemented zero electron mass versions of both electrostatic and electromagnetic models. For all variants the STORM code solves a continuity equation

$$\frac{\partial n}{\partial t} = -\nabla \cdot \left(\mathbf{b}\, n\, v_{e\parallel}\right) - \frac{1}{B}\mathbf{b} \times \nabla\phi \cdot \nabla n$$
$$+ \nabla \times \left(\frac{\mathbf{b}}{B}\right) \cdot \nabla p_e - n\nabla \times \left(\frac{\mathbf{b}}{B}\right) \cdot \nabla\phi + S_n$$
$$+ \nabla \cdot \left(D_\perp \nabla_\perp n\right), \tag{B.1}$$

where S_n is the density source; an electron temperature equation

$$\frac{\partial T_e}{\partial t} = -v_{e\parallel}\partial_\parallel T_e - \frac{1}{B}\mathbf{b} \times \nabla\phi \cdot \nabla T_e - \frac{2}{3n}\nabla \cdot \left(\mathbf{b}\, q_{e\parallel}\right)$$
$$+ \frac{2T_e}{3n}\nabla \times \left(\frac{\mathbf{b}}{B}\right) \cdot \left(\nabla p_e - n\nabla\phi + \frac{5}{2}n\nabla T_e\right)$$
$$- \frac{2T_e}{3}\nabla \cdot \left(\mathbf{b}\, v_{e\parallel}\right) + \frac{2}{3}\left(v_{i\parallel} - v_{e\parallel}\right)\left(\eta J_\parallel - \frac{0.71}{e}\partial_\parallel T\right)$$
$$+ \frac{2S_E}{3n} + \frac{v_{e\parallel}^2 S_n}{3em_e n} - \frac{T_e S_n}{n} + \frac{2}{3n}\nabla \cdot \left(\kappa_{e\perp}\nabla_\perp T_e\right), \tag{B.2}$$

where the parallel electron thermal conduction is $q_{e\parallel} = -3.16enT\tau_{\text{ei}}\partial_\parallel T/m_e - 0.71nT\left(v_{i\parallel} - v_{e\parallel}\right)$ and S_E is the energy source; and a vorticity equation

$$\frac{\partial\Omega}{\partial t} = -\nabla \cdot \left(\frac{1}{B}\mathbf{b} \times \nabla\phi \cdot \nabla\boldsymbol{\omega}\right) - \nabla \cdot \left(\partial_\parallel \left(v_{i\parallel}\boldsymbol{\omega}\right)\right)$$
$$+ \nabla \cdot \left(\mathbf{b}J_\parallel\right) + e\nabla \times \left(\frac{\mathbf{b}}{B}\right) \cdot \nabla p_e + \nabla \cdot \left(\mu_\Omega \nabla_\perp \Omega\right), \tag{B.3}$$

where for this non-linear model we use a generalised vorticity without Boussinesq approximation $\Omega = \nabla \cdot \boldsymbol{\omega}$, $\boldsymbol{\omega} = en\nabla_\perp\phi/\Omega_i B$. The perpendicular dissipation parameters $D_\perp$, $\kappa_\perp$ and μ_Ω take small, classical values as described in [41] and do not have a significant influence on the results, being retained mainly to ensure numerical stability.

The differences between variants are in the parallel momentum equations. We use the parameters α and μ, where

$$\alpha = \begin{cases} 0 & \text{for electrostatic cases,} \\ 1 & \text{for electromagnetic cases,} \end{cases}$$

$$\mu = \begin{cases} 0 & \text{for zero electron mass,} \\ 1 & \text{for finite electron mass,} \end{cases}$$

to express the ion parallel momentum equation as

$$\frac{\partial}{\partial t}\left(v_{i\parallel} + \mu\alpha\frac{e}{m_i}A_\parallel\right) = -v_{i\parallel}\partial_\parallel v_{i\parallel} - \frac{1}{B}\mathbf{b}\times\nabla\phi\cdot\nabla v_{i\parallel}$$
$$- \frac{e}{m_i}\partial_\parallel\phi - \frac{e\eta}{m_i}J_\parallel + \frac{0.71}{m_i}\partial_\parallel T - \frac{v_{i\parallel}S_n}{n}$$
(B.4)

and Ohm's law as

$$\mu\frac{\partial}{\partial t}\left(v_{e\parallel} - \alpha\frac{e}{m_e}A_\parallel\right)$$
$$= -\mu\left(v_{e\parallel}\partial_\parallel v_{e\parallel} + \frac{1}{B}\mathbf{b}\times\nabla\phi\cdot\nabla v_{e\parallel} - \frac{v_{e\parallel}S_n}{n}\right)$$
$$- \frac{e}{m_e n}\partial_\parallel p_e + \frac{e}{m_e}\partial_\parallel\phi + \frac{e\eta}{m_e}J_\parallel - \frac{0.71}{m_e}\partial_\parallel T.$$
(B.5)

STORM uses Ampère's law in the form

$$\nabla_\perp^2 A_\parallel = -\mu_0 J_\parallel$$
(B.6)

B.2. Isolated filament simulation setup

The simulations are performed in slab geometry with a constant magnetic field of $B = 0.5$ T. The effect of non-uniform magnetic field is retained only through the curvature terms $\nabla\times(\mathbf{b}/B)\cdot\nabla = 2(BR_c)^{-1}\nabla_z$ with radius of curvature $R_c = 1.5$ m. The spatial grid has $240\times64\times128$ points in the radial, parallel and binormal directions x, y and z. The grid size is $L_x\times L_\parallel\times L_z = 93.75\rho_{s0}\times11000\rho_{s0}\times50\rho_{s0}$, where $\rho_{s0} = \rho_s(T = 20$ eV$) = 1.29$ mm, giving a perpendicular grid spacing of $0.391\rho_{s0}$ and a parallel grid spacing of $172\rho_{s0}$. The parallel boundaries use Bohm sheath boundary conditions: $v_{i\parallel,sh} = \pm\sqrt{eT_{sh}/(m_i + m_e)}$, $v_{e\parallel,sh} = \pm\sqrt{m_i eT_{sh}/2\pi m_e(m_i + m_e)}\exp(-\phi_{sh}/T_{sh})$ and $q_{e\parallel,sh} = (2 - 0.5\ln(2\pi m_e/m_i))n_{sh}T_{sh}v_{e\parallel,sh} - 5p_{e,sh}v_{e\parallel,sh}/2 - m_e n_{sh}v_{e\parallel,sh}^3/2e$. The perpendicular boundaries are far enough from the filament to have little effect: Neumann boundary conditions are used in the radial direction for all variables except ϕ, which is set equal to its background value; periodic boundary conditions are used in the binormal direction.

A steady background plasma is created by balancing the sinks at the sheaths with sources $S_n = S_{n0}\left[\exp(20(y/L_\parallel - 1/2)) + \exp(-20(y/L_\parallel + 1/2))\right]$ and $S_E = S_{E0}\exp(-10|y|/L_\parallel)$, whose prefactors are adjusted so that the density and temperature at the mid-point of the simulation domain are 8×10^{18} m^{-3} and 20 eV.

The filament simulations are run by adding a density perturbation on top of the background

$$\Delta_n = A\frac{1}{2}\left[1 - \tanh\left(\left(\frac{y - L_\parallel/4}{L_\parallel/8}\right)\right)\right]$$
$$\times\frac{1}{2}\left[1 - \tanh\left(\frac{-y - L_\parallel/4}{L_\parallel/8}\right)\right]\exp\left(-\frac{x^2 + z^2}{\delta_\perp^2}\right),$$
(B.7)

with amplitude $A = 1.6\times10^{19}$ m^{-3} and perpendicular width $\delta_\perp = 5\rho_{s0}$, and allowing the simulation to evolve for $1000\Omega_i^{-1} = 41.5$ μs.

ORCID iDs

B D Dudson ⬤ https://orcid.org/0000-0002-0094-4867
J T Omotani ⬤ https://orcid.org/0000-0002-3156-8227

References

[1] Braginskii S I 1965 Transport processes in a plasma *Reviews of Plasma Physics* vol 1, ed M A Leontovich (New York: Consultants Bureau) pp 205–311
[2] Buchlin E and Velli M 2007 *Astrophys. J.* **662** 701
[3] van Ballegooijen A A, Asgari-Targhi M, Cranmer S R and DeLuca E E 2011 *Astrophys. J.* **736** 3
[4] Schekochihin A A, Cowley S C and Dorland W 2007 *Plasma Phys. Control. Fusion* **49** A195
[5] Rosenbluth M N, Monticello D A, Strauss H R and White R B 1976 *Phys. Fluids* **19** 1987
[6] Strauss H R 1976 *Phys. Fluids* **19** 134
[7] Strauss H R 1982 *Nucl. Fusion* **22** 893
[8] Mikhailovskii A B and Tsypin V S 1984 *Beitr. Plasmaphys.* **24** 335–54
[9] Drake J F and Anthonsen Jr T M 1984 *Phys. Fluids* **27** 898
[10] Hazeltine R D and Meiss J D 1985 *Phys. Rep.* **121** 1–164
[11] Hsu C T, Hazeltine R D and Morrison P J 1986 *Phys. Fluids* **29** 1480
[12] Hazeltine R D, Hsu C T and Morrison P J 1987 *Phys. Fluids* **30** 3204
[13] Pfirsch D and Correa-Restrepo D 1996 *Plasma Phys. Control. Fusion* **38** 71–101
[14] Scott B 1997 *Plasma Phys. Control. Fusion* **39** 1635
[15] Kruger S E, Hegna C C and Callen J D 1998 *Phys. Plasmas* **5** 4169
[16] Simakov A N and Catto P J 2003 Drift-ordered fluid equations for field-aligned modes in low-β collisional plasma with equilibrium pressure pedestals *Phys. Plasmas* **10** 4744–57
[17] Brizard A J 2005 *Phys. Plasmas* **12** 092302
[18] Ramos J J 2005 *Phys. Plasmas* **12** 052102
[19] Reiser D 2012 *Phys. Plasmas* **19** 072317
[20] Rognlien T D, Xu X Q and Hindmarsh A C 2002 *J. Comput. Phys.* **175** 249–68
[21] Schnack D D, Barnes D C, Brennan D P, Hegna C C, Held E, Kim C C, Kruger S E, Pankin A Y and Sovinec C R 2005 *Bull. Am. Phys. Soc.* **50** 137
[22] Jardin S C 2012 *J. Comput. Phys.* **231** 822–38
[23] Xu X Q, Umansky M V, Dudson B and Snyder P B 2008 Boundary plasma turbulence simulations for tokamaks *Comm. in Comput. Phys.* **4** 949–79 Report LLNL-JRNL–404082
[24] Umansky M V, Xu X Q, Dudson B, LoDestro L L and Myra J R 2008 Status and verification of edge plasma turbulence code bout *Comp. Phys. Comm.* **180** 887–903
[25] Dudson B D *et al* 2009 *Comp. Phys. Comm.* **180** 1467–80
[26] Ricci P, Halpern F D, Jolliet S, Loizu J, Mosetto A, Fasoli A, Furno I and Theiler C 2012 *Plasma Phys. Control. Fusion* **54** 124047
[27] Tamain P, Ghendrih P, Tsitrone E, Grandgirard V, Garbet X, Sarazin Y, Serre E, Ciraolo G and Chiavassa G 2010 *J. Comput. Phys.* **229** 361–78
[28] Easy L, Militello F, Omotani J, Dudson B, Havlíčková E, Tamain P, Naulin V and Nielsen A H 2014 Three dimensional simulations of plasma filaments in the scrape off layer: a comparison with models of reduced dimensionality *Phys. Plasmas* **21** 122515
[29] Cohen B I, Umansky M V, Nevins W M, Makowski M A, Boedo J A, Rudakov D L, McKee G R, Yan Z and Growbner R J 2013 *Phys. Plasmas* **20** 055906

[30] Lee W, Umansky M V, Angus J R and Krasheninnikov S I 2015 *Phys. Plasmas* **22** 012505

[31] Angus J R and Umansky M V 2014 *Phys. Plasmas* **21** 012514

[32] Walkden N R, Dudson B D, Easy L, Fishpool G and Omotani J T 2015 *Nucl. Fusion* **55** 113022

[33] Helander P and Sigmar D J 2005 *Collisional Transport in Magnetized Plasmas* vol 4 (Cambridge: Cambridge University Press)

[34] Hasegawa A and Uberoi C 1982 Alfven wave. DOE Critical Review Series *Technical Report DOE/TIC-11197* (Washington, DC, USA): Department of Energy, Office of Technical Information)

[35] Lee W W 1987 Gyrokinetic particle simulation model *J. Comput. Phys.* **72** 243–69

[36] McMillan B F 2020 Is it necessary to resolve the Debye length in standard or δf PIC codes? *Phys. Plasmas* **27** 052106

[37] Elmore S *et al* the MAST Team 2012 Upstream and divertor ion temperature measurements on MAST by retarding field energy analyser *Plasma Phys. Control. Fusion* **54** 065001

[38] Allan S Y, Elmore S, Fishpool G and Dudson B the MAST Team and the EUROFusion MST1 Team 2016 Ion temperature measurements of l-mode filaments in MAST by retarding field energy analyser *Plasma Phys. Control. Fusion* **58** 045014

[39] Stix T H 1992 *Waves in Plasmas* (New York: Springer Science & Business Media)

[40] Riva F, Militello F, Elmore S, Omotani J T, Dudson B and Walkden N R 2019 and the MAST team. Three-dimensional plasma edge turbulence simulations of the mega ampere spherical tokamak and comparison with experimental measurements *Plasma Phys. Control. Fusion* **61** 095013

[41] Ahmed S, Omotani J T, Newton S L and Birch J 2021 STORM modelling of SOL filament behaviour with hot ions (in preparation)

[42] Omotani J T, Dudson B, Newton S L and Birch J 2021 On Ohm's law in reduced plasma fluid model (available at: https://doi.org/10.5281/zenodo.5525078)

[43] Hindmarsh A C *et al* 2005 SUNDIALS: suite of nonlinear and differential/algebraic equation solvers *ACM Trans. Math. Softw.* **31** 363–96

[44] Lewy H, Friedrichs K and Courant R 1928 Über die partiellen differenzengleichungen der mathematischen physik *Mathematische Annalen* **100** 32–74

[45] Hoare D, Militello F, Omotani J T, Riva F, Newton S, Nicholas T, Ryan D, and Walkden N R 2019 Dynamics of scrape-off layer filaments in high β plasmas *Plasma Phys. Control. Fusion* **61** 105013